CRYSTAL GROWTH & DESIGN

pubs.acs.org/crystal

Article

Rational Design of Bioinspired Nanocomposites with Tunable Catalytic Activity

Hans C. Hendrikse, Alejo Aguirre, Arno van der Weijden, Anne S. Meeussen, Fernanda Neira D'Angelo,* and Willem L. Noorduin*

Cite This: *Cryst. Growth Des.* 2021, 21, 4299−4304

Read Online

ACCESS | Metrics & More | Article Recommendations | Supporting Information

ABSTRACT: Biological assembly processes offer inspiration for ordering building blocks across multiple length scales into advanced functional materials. Such bioinspired strategies are attractive for assembling supported catalysts, where shaping and structuring across length scales are essential for their performance but still remain tremendously difficult to achieve. Here, we present a simple bioinspired route toward supported catalysts with tunable activity and selectivity. We coprecipitate shape-controlled nanocomposites with large specific surface areas of barium carbonate nanocrystals that are uniformly embedded in a silica support. Subsequently, we exchange the barium carbonate to cobalt while preserving the nanoscopic layout and microscopic shape, and demonstrate their catalytic performances in the Fischer−Tropsch synthesis as a case study. Control over the crystal size between 10 and 17 nm offers tunable activity and selectivity for shorter (C_5−C_{11}) and longer (C_{20+}) hydrocarbons, respectively. Hence, these results open simple, versatile, and scalable routes to tunable and highly reactive bioinspired catalysts.

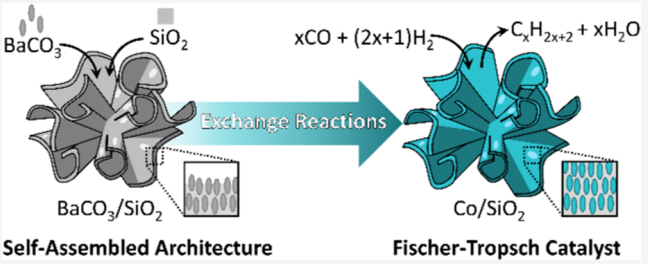

1. INTRODUCTION

The exquisite complexity and hierarchical structuring of biominerals offer an inexhaustible source of inspiration for the assembly of new materials with advanced functionalities.[1−5] In particular, bioinspired self-assembly can be exploited for hierarchical ordering of amorphous and crystalline substances in functional nanocomposites, while the inherent autonomous character of self-assembly is advantageous for straightforward upscaling.[6−26] Consequently, bioinspired nanocomposites have already been applied in fields such as robotics, sensing, and optics,[14,27−29] yet the full potential of self-assembly for advanced materials remains untapped.

Specifically, such bioinspired strategies could potentially be exploited in the field of catalysis, where shaping and structuring across length scales is essential for catalytic performance.[30−35] Of particular interest are supported catalysts consisting of metallic nanosized crystals dispersed on the surface of a porous (typically ceramic) support. Ideally, supported catalysts have the following properties: (i) a large macroscale surface and nanoscale porosity for maximum accessibility of the reagents and products; (ii) high metal loadings for high reactivity; (iii) well-controlled nanocrystal size and size distributions for optimal catalytic activity and selectivity; and (iv) uniform dispersion of the nanocrystals on the surface of the support to prevent undesirable agglomeration of the nanocrystals, which may impede both the activity and selectivity of the catalyst over time. Despite tremendous progress in nanoparticle fabrication and catalyst preparation methods,[32−40] ceding control over all but the starting materials, leaves little opportunity to fine-tune crystal sizes, let alone uniformly distribute nanocrystals in shape-controlled supported catalysts.

An attractive system to overcome this limitation is the bioinspired coprecipitation of barium carbonate ($BaCO_3$) nanocrystals and amorphous silica (SiO_2).[15−20] Here, the crystallization of $BaCO_3$ is steered by the precipitation of SiO_2 through an acid-regulated feedback mechanism, resulting in intricate and controllable microshapes (Figure 1).[15−18] This system inherently produces the desired material properties for supported catalysts: (i) programmable microshapes—including coral-like geometries that maximize the surface area; (ii) a nanocomposite layout with a high metal-to-silica molar ratio of 4:1; (iii) nanocrystals of ca. 20 nm that are (iv) uniformly dispersed in a silica support. Moreover, inspired by naturally occurring fossilization processes and nanocrystal fabrication,[21,22,41−43] the chemical composition of the nanocrystals can be completely overhauled using ion-exchange reactions while preserving the microscopic shape and submicron features of the original nanocomposite.[23,24] These insights highlight an enormous potential for the assembly of bioinspired functional

Received: February 11, 2021
Revised: July 2, 2021
Published: July 14, 2021

https://doi.org/10.1021/acs.cgd.1c00165
Cryst. Growth Des. 2021, 21, 4299−4304

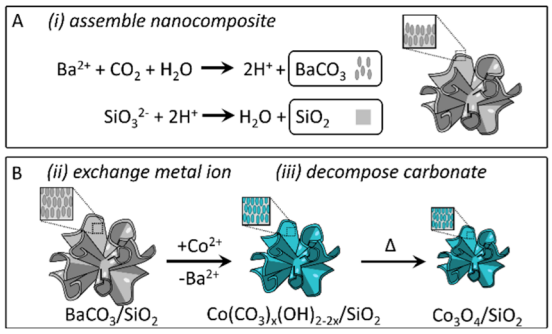

Figure 1. Preparation of catalytic nanocomposites. (A) Coprecipitation of nanocomposites containing $BaCO_3$ nanocrystals and amorphous SiO_2. (B) Nanocrystals of the composites are converted by replacing the Ba^{2+} with Co^{2+} followed by decomposition to Co_3O_4, which serves as the precursor of the Fischer–Tropsch catalyst.[42]

materials and suggest the possibility to integrate desirable catalytic properties into these materials by fine-tuning the assembly/exchange processes.

Here, we demonstrate this potential by converting $BaCO_3/SiO_2$ nanocomposites to cobalt oxide/silica (Co_3O_4/SiO_2) nanocomposites that, upon reductive treatment to Co/SiO_2, become catalysts with tunable activity. In this work, the Fischer–Tropsch synthesis (FTS)[42]—a chemical conversion that receives wide attention for its unique ability to produce high-value hydrocarbons (C_xH_{2x+2}) from cheap feedstocks of hydrogen (H_2) and carbon monoxide (CO)[43−48]—is used as a model reaction to assess the catalytic activity of the bioinspired nanocomposites. Typical FTS catalysts are composed of nanoparticles of Fe or Co immobilized on porous supports like SiO_2 or Al_2O_3,[49] with the Co nanoparticle size being a key parameter that affects the activity and selectivity of the reaction.[50] Thus, this sensitivity of product distribution on nanocrystal sizes makes the FTS an ideal case study for probing the tunable selectivity of bioinspired nanocomposite catalysts.

2. EXPERIMENTAL SECTION

2.1. Growth of $BaCO_3/SiO_2$ Nanocomposites. A solution of $BaCl_2$ (7.4 g, 30 mM) in 300 mL of water was added to a solution of Na_2SiO_3 (1.6 g, 13 mM) in 1200 mL of water. This solution was poured in a metal tray (30 × 50 × 10 cm^3) while keeping at least 1 cm of depth to the solution. The solution was left for 1.5 h with the tray covered with a perforated cardboard lid. The resulting nanocomposites were separated from the solution via vacuum filtration.

2.2. Exchange to $Co(CO_3)_x(OH)_{2-2x}$. Cobalt nitrate hexahydrate ($Co(NO_3)_2$) (11.6 g, 40 mM) was dissolved in 200 mL of demineralized water. $BaCO_3/SiO_2$ nanocomposites were placed in this solution using a spatula while gently stirring the solution to spread the nanocomposites. Afterward, the resulting purple nanocomposites were separated from the solution using vacuum filtration and washed with demineralized water followed by acetone.

2.3. Exchange to Co_3O_4. An alumina boat containing $Co(CO_3)_x(OH)_{2-2x}/SiO_2$ nanocomposites was placed in an open single zone tube furnace and heated to 530, 560, 590, 620, or 650 °C for 4 h. Afterward, the resulting black nanocomposites were retrieved by passively cooling the furnace to room temperature and retrieving the alumina boat.

2.4. Catalytic Analysis. The catalysts were tested for the FTS at 20 bar, 220 °C, H_2/CO = 2/1 and gas hourly space velocity (GHSV) = 320 mL g_{cat}^{-1} min^{-1}. The nanocomposite catalysts (160 mg) were diluted with SiC (1:6) and located in a 10 mm diameter Hastelloy reactor. Above the catalysts and next to the reactor inlet, a bed of SiC was placed to ensure that the gases were preheated. The reactor was placed in an oven (Carbolite Gero), and the temperature was measured with a thermocouple at the reactor exit and one thermocouple inserted in the SiC bed. The liquid products were collected in a hot-trap at the reactor exit, while the gases flowed through a heated line at 250 °C, toward the gas chromatograph (see Section S12 for details).

3. RESULTS AND DISCUSSION

Our strategy comprises three steps (Figure 1): (1) the nanocomposite is assembled via coprecipitation of $BaCO_3$ and SiO_2; (ii) $BaCO_3$ is replaced with cobalt via cation exchange, and (iii) the cobalt is decomposed to yield the desired cobalt oxide (Co_3O_4) catalyst precursor material while preserving the nanoscale organization and microscopic shape of the original nanocomposite. To demonstrate the shape-preservation, we analyze the same architecture throughout the entire procedure and perform complementary analysis on bulk samples.

In the first step, we program the desired microscopic shape. Ideally, the microscopic shape of the eventual catalyst has a large surface that is well accessible for the reactants and products. To achieve this, we steer the coprecipitation of the original $BaCO_3/SiO_2$ nanocomposite toward coral-like shapes with many extrusions to maximize the surface area of the architecture (for details, see Section S1).[16] Scanning electron microscopy (SEM) confirms the coral-like shape of the resulting nanocomposites (Figure 2A). Consistent with previous reports,[15,16,18] energy-dispersive X-ray spectroscopy (EDS) shows that the nanocomposite has a barium/silicon molar ratio of 4:1 (Figure 2B), with barium crystallizing as

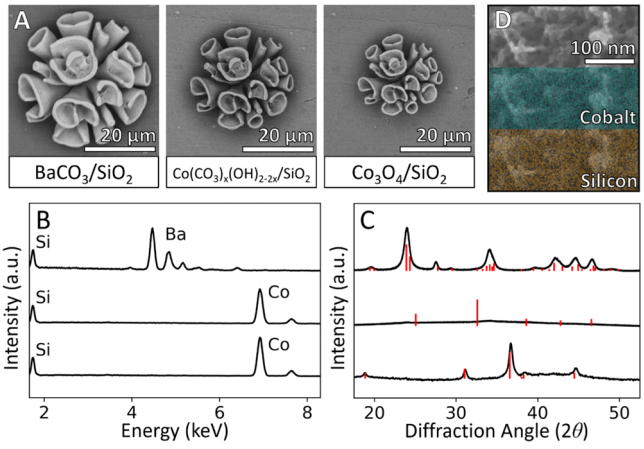

Figure 2. Shape-preserving conversion of $BaCO_3/SiO_2$ to Co_3O_4/SiO_2 nanocomposites. (A) SEM images of self-assembled nanocomposites before exchange (left, $BaCO_3/SiO_2$), after cation exchange (middle, $Co(CO_3)_x(OH)_{2-2x}/SiO_2$), and after decomposition (right, Co_3O_4/SiO_2). (B) EDS analysis showing the presence of barium and silica in the initial $BaCO_3/SiO_2$ nanocomposite (top), the replacement of Ba^{2+} for Co^{2+} after the cation exchange (middle), and the preservation of the metal-to-silicon ratio after decomposition (bottom). (C) XRD data of the initial $BaCO_3$ (top, orthorhombic), intermediate $Co(CO_3)_x(OH)_{2-2x}$ (middle, amorphous), and Co_3O_4 (bottom, cubic). Reference lines in red show peaks measured in literature (COD 1000033, COD 1548825, and ICSD 27498 respectively, see Sections S1–S5 for details). (D) High-resolution SEM image of the Co_3O_4/SiO_2 nanocomposite surface (top), with corresponding EDS overlay showing the distribution of cobalt (cyan, middle) and silicon (brown, bottom).

https://doi.org/10.1021/acs.cgd.1c00165
Cryst. Growth Des. 2021, 21, 4299−4304

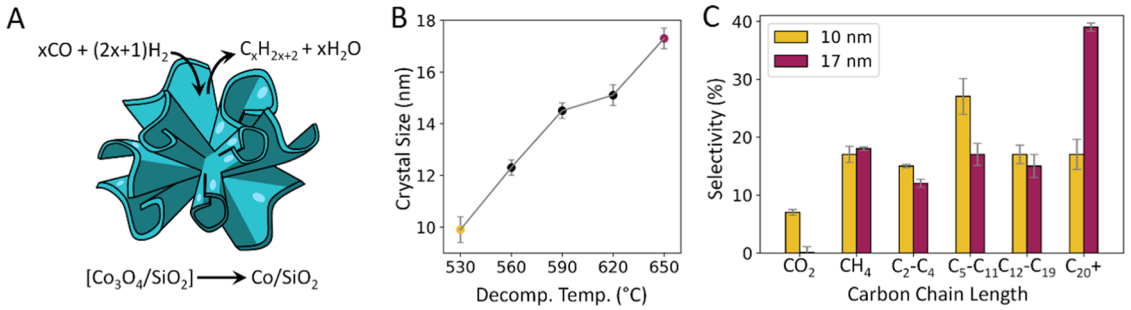

Figure 3. Self-assembled Co_3O_4/SiO_2 nanocomposites for tunable catalysis of the Fischer–Tropsch synthesis. (A) FTS reaction on Co_3O_4/SiO_2 that is reduced to Co/SiO_2 in the reactor. The hydrocarbon chain length C_x is determined by the Co_3O_4 crystal size. (B) Modifying the decomposition temperature in step (iii) (Figure 1B) enables customization of the Co_3O_4 nanocrystal size (C) FTS reaction products for Co_3O_4 crystal sizes of 10 and 17 nm, showing a preferred formation of C_{5-11} and C_{20+}, respectively.

orthorhombic barium carbonate (witherite) according to X-ray diffraction (XRD) (Figure 2C).

In the second step, the desired cobalt ion is introduced by immersing the nanocomposites in a solution of 5.0 mM $Co(NO_3)_2$ for 50 min (for details, see Sections S3 and S4). EDS confirms the complete exchange of Ba^{2+} with Co^{2+} (Figure 2B). The absence of diffraction peaks in the XRD analysis suggests formation of basic amorphous cobalt carbonate ($Co(CO_3)_x(OH)_{2-2x}$), which is supported by the presence of the carbonate fingerprint peak in IR measurements (Figure 2C and Section S13).

Comparing SEM images of the same coral shapes before and after conversion shows that the overall shape shrinks by ca. 60%, which may partially be attributed to the decrease in ionic radius from the exchange of Ba^{2+} (149 pm) to Co^{2+} (80 pm).[51] Despite this dramatic shrinking, the microscopic form and fine details are well-preserved after the conversion (Figure 2A). This demonstrates the potential of the nanocomposite layout for shape-preserving conversion reactions: the nanocrystals offer high chemical reactivity, while the silica matrix provides mechanical stability.[24]

In the third step, the resulting cobalt carbonate phase is thermally decomposed into Co_3O_4 by heating the nanocomposites to 650 °C for 4 h (for details see Section S5). XRD and EDS confirm complete conversion toward the cubic crystalline phase of Co_3O_4 with preservation of the 4:1 metal:silicon molar ratio (Figure 2B,C). Furthermore, high-resolution SEM and EDS mapping (Figure 2D) reveals that the nanocomposite surface is highly porous, with a uniformly dispersed elemental distribution of cobalt and silicon (Figure 2D and Section S6). During the overall conversion of $BaCO_3$ to Co_3O_4, the volume of the crystal lattice shrinks by more than 70%. Indeed, comparing the microshape before and after the conversion shows a shrinking of ca. 80% (Figure 2A, see Section S9 for details). The nanocomposite layout thus translates the volume changes at the atomic scale to the microscopic shrinking. Consequently, despite dramatic shrinking at atomic length scales, the final Co_3O_4/SiO_2 microshape is geometrically indistinguishable from the original $BaCO_3/SiO_2$ form, and even sub-micrometer details and the nanocomposite layout remain preserved.

We quantify the available surface for catalysis by determining the BET surface area (S_{BET}) and pore distribution of the Co_3O_4/SiO_2 nanocomposite using a Micromeritics Tristar II. We find a S_{BET} of 36.3 m^2/g and an average pore size of 6.6 nm (Section S12). This material presents a moderate internal surface area and large mesoporosity, and is thus adequate for catalysis. We explore the functionality potential of this shape-preserving conversion route by testing the catalytic performance of Co_3O_4/SiO_2 nanocomposites for FTS, forming hydrocarbons with various carbon chain lengths (C_xH_{2x+2}) from hydrogen (H_2) and carbon monoxide (CO) (Figure 3A).[45−47,50] The ideal hydrocarbon chain length (C_x) varies based on its intended application: shorter chains are favored for naphtha and gasoline ($x = 5-11$),[46] while longer chains are ideal for waxes and lubricant oils ($x > 20$).[47] Since the chain length depends on the size of the cobalt crystals,[50] it is highly desirable to control the crystal size of the Co_3O_4 crystals within the catalyst.

We tune the crystal size within the Co_3O_4/SiO_2 nanocomposites by inducing sintering of the crystals during the decomposition in step (iii) of our assembly scheme (Figure 1B). To this aim, we perform decomposition processes at different temperatures and determine the crystal size from X-ray powder diffractograms using the Scherrer equation (see Supporting Information). Consistent with previously observed sintering,[52,53] we observe an almost linear increase in crystal sizes from ca. 10 nm (Co_3O_4 (10 nm)/SiO_2) to ca. 17 nm (Co_3O_4 (17 nm)/SiO_2) for temperatures ranging from 530 to 650 °C (Figure 3B). Remarkably, the microscopic geometry of the nanocomposites remains preserved, while the nanoscopic crystal size can be tailored precisely over a wide range of sizes.

We scale up the fabrication of the nanocomposites to test the catalytic performance (Section S2). To this end, we take advantage of the autonomous nature of our bottom-up assembly process to scale the nanocomposite assembly by >500-fold from a few micrograms of architectures on a substrate up to multiple grams of bulk materials. Specifically, we use commercial kitchen trays to increase the reaction volume and maximize the air–liquid interface for CO_2 uptake (see Sections S2 and S11 for details). XRD, EDS, and SEM analyses confirm complete conversion to Co_3O_4 with preservation of the nanocomposite layout and tunable nanoparticle size in these scaled-up reactions (Section S11).

We perform the Fischer–Tropsch synthesis with Co_3O_4 (17 nm)/SiO_2 nanocomposites. The nanocomposites are placed in a gas flow reactor and are reduced to the active metal cobalt catalyst with H_2 (10% in N_2 flow rate of 50 mL min^{-1}) at 400 °C. Then, the reactor is cooled down to the reaction temperature of 200 °C. FTS is initiated by flowing H_2, CO, and N_2 (with a ratio of 6:3:1) into the reactor at 20 bar and a gas hourly space velocity (GHSV) of 320 mL $gcat^{-1}$ min^{-1}. The reaction progress is followed using real-time online gas chromatography. We observe an initial conversion of 13% and

https://doi.org/10.1021/acs.cgd.1c00165
Cryst. Growth Des. 2021, 21, 4299−4304

a steady-state conversion rate of 5% with a turnover frequency (TOF) of 6.2 × 10^{-3} s^{-1} (see Section S12 for details), a performance which is comparable with traditionally-prepared state-of-the-art catalysts.[50,54,55] Remarkably, the reaction predominantly produces long carbon chains, with 40% of the products having a chain length of C_{20+}, which is a desired attribute in FTS catalysts, commonly associated with large and uniformly distributed nanocrystals.[47,50] Hence, these findings demonstrate the functionality potential of these self-assembled nanocomposites for selectively catalyzing FTS.

According to the current understanding of FTS cobalt catalysts, smaller nanocrystals catalyze the formation of shorter hydrocarbon chains with respect to larger crystals, while the effects of crystal size on reaction rate (TOF) depend on the size range.[45,46,50] Most studies agree that TOF increases with the crystal size up to ca. 6−10 nm and remains nearly invariant with larger crystals, while others report a negative effect of TOF for even larger crystals of ca. 10−15 nm.[50] Thus, to further assess the functionality potential of the self-assembled nanocomposites, we tune the catalytic selectivity and activity of the FTS reaction by tailoring the nanocrystal size within the nanocomposite. To this aim, we decrease the crystal size of the Co_3O_4/SiO_2 nanocomposites from 17 to 10 nm by performing the decomposition in step (iii) at 530 °C (Figure 3B), and perform the FTS under identical conditions. Consistent with previous reports,[50] the decrease in crystal size (above 10 nm) results in an increase of the initial conversion from 13 to 25%, a steady-state conversion rate from 5 to 15%, and a TOF increase from 6.2 × 10^{-3} to 9.8 × 10^{-3} s^{-1}. Furthermore, as expected, the decrease of the nanocrystal size shifts the selectivity of these catalysts to form predominately shorter carbon chains, with 27% of the products as C_{5-11} while only 17% of the products have a chain length of C_{20+} (Figure 3C). Thus, our self-assembly scheme enables customization of the nanoscopic crystal size within the composites for straightforwardly tuning of the catalytic activity of the FTS.

4. CONCLUSIONS AND OUTLOOK

Here, we introduce a scalable bioinspired strategy for assembling supported catalysts with well-distributed nanocrystals and independently tunable nanocrystal size. We program the microscopic shape of the catalyst during the coprecipitation of $BaCO_3/SiO_2$, which also automatically distributes the $BaCO_3$ nanocrystals uniformly in the silica matrix with a high metal loading. Subsequently, we fine-tune the nanoscale crystal size by modulating the reaction conditions during the conversion of $BaCO_3$ into the desired cobalt oxide (Co_3O_4) catalyst precursor, while preserving the nanocomposite layout and microscopic shape. We further prove the versatility and application potential of these self-assembled nanocomposites with tunable catalytic activity.

Our assembly/conversion strategy enables further customization of the catalysts. We focused on converting the complete interior of the composites. However, since only the outer parts participate in the catalysis, it may be favorable to perform partial conversion to reduce the metal loading while preserving the catalytic activity. Moreover, selective conversion may enable the spatial positioning of multiple catalytic materials for cascade reactions.[56] We foresee that our conversion reaction scheme can straightforwardly be extended to calcium carbonate as a starting material, thus gaining access to the vast catalogue of biological calcium carbonate architectures to leverage nature's exquisite morphogenesis strategies with state-of-the-art artificial catalytic performance. Hence, bioinspired self-assembly strategies may offer previously unimaginable control and tunability for shaping and structuring catalysts for a myriad of catalytic reactions.

■ ASSOCIATED CONTENT

Supporting Information

The Supporting Information is available free of charge at https://pubs.acs.org/doi/10.1021/acs.cgd.1c00165.

Synthesis methods and equipment used (PDF)

■ AUTHOR INFORMATION

Corresponding Authors

Fernanda Neira D'Angelo − *Laboratory of Chemical Reactor Engineering, Department of Chemical Engineering and Chemistry, Eindhoven University of Technology, 5600 MB Eindhoven, The Netherlands;* orcid.org/0000-0001-8599-2800; Email: M.F.Neira.dAngelo@tue.nl.

Willem L. Noorduin − *AMOLF, 1098 XG Amsterdam, The Netherlands; Van't Hoff Institute for Molecular Sciences, University of Amsterdam, 1090 GD Amsterdam, The Netherlands;* orcid.org/0000-0003-0028-2354; Email: W.Noorduin@amolf.nl

Authors

Hans C. Hendrikse − *AMOLF, 1098 XG Amsterdam, The Netherlands*

Alejo Aguirre − *Laboratory of Chemical Reactor Engineering, Department of Chemical Engineering and Chemistry, Eindhoven University of Technology, 5600 MB Eindhoven, The Netherlands;* Present Address: Instituto de Desarrollo Tecnológico para la Industria Química (INTEC), Universidad Nacional del Litoral, CONICET, Güemes 3450, S3000-GLN Santa Fe, Argentina

Arno van der Weijden − *AMOLF, 1098 XG Amsterdam, The Netherlands*

Anne S. Meeussen − *AMOLF, 1098 XG Amsterdam, The Netherlands; Leiden Institute of Physics, Leiden University, 2333 CA Leiden, The Netherlands*

Complete contact information is available at: https://pubs.acs.org/10.1021/acs.cgd.1c00165

Author Contributions

The manuscript was written through contributions of all authors.

Notes

The authors declare no competing financial interest.

■ ACKNOWLEDGMENTS

This work is part of the Vernieuwingsimpuls Vidi research program "Shaping up materials" with project number 016.Vidi.189.083, which is partly financed by the Dutch Research Council (NWO). This work is furthermore supported by the Netherlands Center for Multiscale Catalytic Energy Conversion (MCEC), an NWO Gravitation program funded by the Ministry of Education, Culture and Science of the government of the Netherlands. The authors thank Serena Poto for performing BET measurements.

ABBREVIATIONS

XRD, X-ray diffraction; EDS, energy-dispersive X-ray spectroscopy; SEM, scanning electron microscopy; IR, infrared spectroscopy

REFERENCES

(1) Jiang, W.; Qu, Z.; Kumar, P.; Vecchio, D.; Wang, Y.; Ma, Y.; Bahng, J. H.; Bernardino, K.; Gomes, W. R.; Colombari, F. M.; Lozada-Blanco, A.; Veksler, M.; Marino, E.; Simon, A.; Murray, C.; Muniz, S. R.; de Moura, A. F.; Kotov, N. A. Emergence of complexity in hierarchically organized chiral particles. *Science* **2020**, *368*, 642−648.

(2) Aizenberg, J.; Weaver, J. C.; Thanawala, M. S.; Sundar, V. C.; Morse, D. E.; Fratzl, P. Materials science: Skeleton of euplectella sp.: Structural hierarchy from the nanoscale to the macroscale. *Science* **2005**, *309*, 275−278.

(3) Mann, S.; Ozin, G. A. Synthesis of inorganic materials with complex form. *Nature* **1996**, *382*, 313−318.

(4) Meldrum, F. C.; Cölfen, H. Controlling mineral morphologies and structures in biological and synthetic systems. *Chem. Rev.* **2008**, *108*, 4332−4432.

(5) Lowenstam, H. A.; Weiner, S. *On Biomineralization*; Oxford University Press: New York, 1989.

(6) Eder, M.; Amini, S.; Fratzl, P. Biological composites—complex structures for functional diversity. *Science* **2018**, *362*, 543−547.

(7) Begley, M. R.; Gianola, D. S.; Ray, T. R. Bridging functional nanocomposites to robust macroscale devices. *Science* **2019**, *364*, No. eaav4299.

(8) Bargardi, F. L.; Le Ferrand, H.; Libanori, R.; Studart, A. R. Bio-inspired self-shaping ceramics. *Nat. Commun.* **2016**, *7*, No. 13912.

(9) Shevchenko, E. V.; Talapin, D. V.; Kotov, N. A.; O'Brien, S.; Murray, C. B. Structural diversity in binary nanoparticle superlattices. *Nature* **2006**, *439*, 55−59.

(10) Wegst, U. G. K.; Bai, H.; Saiz, E.; Tomsia, A. P.; Ritchie, R. O. Bioinspired structural materials. *Nat. Mater.* **2015**, *14*, 23−36.

(11) Whitesides, G. M.; Grzybowski, B. Self-assembly at all scales. *Science* **2002**, *295*, 2418−2421.

(12) Singh, G.; Chan, H.; Baskin, A.; Gelman, E.; Repnin, N.; Král, P.; Klajn, R. Self-assembly of magnetite nanocubes into helical superstructures. *Science* **2014**, *345*, 1149−1153.

(13) Vogel, N.; Retsch, M.; Fustin, C. A.; Del Campo, A.; Jonas, U. Advances in Colloidal Assembly: The Design of Structure and Hierarchy in Two and Three Dimensions. *Chem. Rev.* **2015**, *115*, 6265−6311.

(14) Studart, A. R. Towards high-performance bioinspired composites. *Adv. Mater.* **2012**, *24*, 5024−5044.

(15) García-ruiz, J. M.; Melero-García, E.; Hyde, S. T. Morphogenesis of Self-Assembled Nanocrystalline Materials of Barium Carbonate and Silica. *Science* **2009**, *323*, 362−366.

(16) Noorduin, W. L.; Grinthal, A.; Mahadevan, L.; Aizenberg, J. Rationally designed complex, hierarchical microarchitectures. *Science* **2013**, *340*, 832−837.

(17) Kaplan, C. N.; Noorduin, W. L.; Ling, L.; Sadza, R.; Folkertsma, L.; Aizenberg, J.; Mahadevan, L. Controlled growth and form of precipitating microsculptures. *Science* **2017**, *355*, 1395−1399.

(18) Knoll, P.; Steinbock, O. Inorganic Reactions Self-organize Life-like Microstructures Far from Equilibrium. *Isr. J. Chem.* **2018**, *58*, 682−692.

(19) Opel, J.; Wimmer, F. P.; Kellermeier, M.; Cölfen, H. Functionalisation of silica-carbonate biomorphs. *Nanoscale Horiz.* **2016**, *1*, 144−149.

(20) Helmbrecht, L.; Tan, M.; Röhrich, R.; Bistervels, M. H.; Ortiz Kessels, B.; Koenderink, A. F.; Kahr, B.; Noorduin, W. L. Directed Emission from Self-Assembled Microhelices. *Adv. Funct. Mater.* **2020**, *30*, No. 1908218.

(21) Putnis, A. Why mineral interfaces matter. *Science* **2014**, *343*, 1441−1442.

(22) Bao, Z.; Weatherspoon, M. R.; Shian, S.; Cai, Y.; Graham, P. D.; Allan, S. M.; Ahmad, G.; Dickerson, M. B.; Church, B. C.; Kang, Z.; Abernathy, H. W., III; Summers, C. J.; Liu, M.; Sandhage, K. H. Chemical reduction of three-dimensional silica micro-assemblies into microporous silicon replicas. *Nature* **2007**, *446*, 172−175.

(23) Holtus, T.; Helmbrecht, L.; Hendrikse, H. C.; Baglai, I.; Meuret, S.; Adhyaksa, G. W. P.; Garnett, E. C.; Noorduin, W. L. Shape-preserving transformation of carbonate minerals into lead halide perovskite semiconductors based on ion exchange/insertion reactions. *Nat. Chem.* **2018**, *10*, 740−745.

(24) Hendrikse, H. C.; van der Weijden, A.; Ronda-Lloret, M.; Yang, T.; Bliem, R.; Shiju, N. R.; van Hecke, M.; Li, L.; Noorduin, W. L. Shape-preserving chemical conversion of architected nanocomposites. *Adv. Mater.* **2020**, *32*, No. 2003999.

(25) Opel, J.; Unglaube, N.; Wörner, M.; Kellermeier, M.; Cölfen, H.; García-ruiz, J. M. Hybrid Biomemetic Materials from Silica/Carbonate Biomorphs. *Crystals* **2019**, *9*, No. 157.

(26) Nakouzi, E.; Steinbock, O. Self-organization in precipitation reactions far from the equilibrium. *Sci. Adv.* **2016**, *2*, No. e1601144.

(27) Pfeifer, R.; Lungarella, M.; Iida, F. Self-Organization, Embodiment, and Biologically Inspired Robotics. *Science* **2007**, *318*, 1088−1093.

(28) McConney, M. E.; Anderson, K. D.; Brott, L. L.; Naik, R. R.; Tsukruk, V. V. Bioinspired Material Approaches to Sensing. *Adv. Funct. Mater.* **2009**, *19*, 2527−2544.

(29) Parker, A. R.; Townley, H. E. Biomimetics of photonic nanostructures. *Nat. Nanotechnol.* **2009**, *230*, 347−353.

(30) García-Ruiz, J. M.; van Zuilen, M. A.; Bach, W. Mineral self-organization on a lifeless planet. *Phys. Life Rev.* **2020**, *34*−*35*, 62−82.

(31) McCollom, T. M.; Seewald, J. S. Abiotic Synthesis of Organic Compounds in Deep-Sea Hydrothermal Environments. *Chem. Rev.* **2007**, *107*, 382−401.

(32) Proppe, A. H.; et al. Bioinspiration in light harvesting and catalysis. *Nat. Rev. Mater.* **2020**, *5*, 828−846.

(33) Munnik, P.; De Jongh, P. E.; De Jong, K. P. Recent Developments in the Synthesis of Supported Catalysts. *Chem. Rev.* **2015**, *115*, 6687−6718.

(34) Campanati, M.; Fornasari, G.; Vaccari, A. Fundamentals in the preparation of heterogeneous catalysts. *Catal. Today* **2003**, *77*, 299−314.

(35) Ertl, G.; Knözinger, H.; Schütz Weitkamp, F. *Handbook of Heterogeneous Catalysis*; Wiley-VCH: Weinheim, Germany, 2008.

(36) Deraz, N. M. The comparative jurisprudence of catalysts preparation methods: I. precipitation and impregnation methods. *J. Ind. Environ. Chem.* **2018**, *2*, 19−21.

(37) Van Dillen, A. J.; Terörde, R. J. A. M.; Lensveld, D. J.; Geus, J. W.; De Jong, K. P. Synthesis of supported catalysts by impregnation and drying using aqueous chelated metal complexes. *J. Catal.* **2003**, *216*, 257−264.

(38) Kanungo, S.; Paunovic, V.; Schouten, J. C.; Neira D'Angelo, M. F. Facile Synthesis of Catalytic AuPd Nanoparticles within Capillary Microreactors Using Polyelectrolyte Multilayers for the Direct Synthesis of H_2O_2. *Nano Lett.* **2017**, *17*, 6481−6486.

(39) Jia, C. J.; Schüth, F. Colloidal metal nanoparticles as a component of designed catalyst. *Phys. Chem. Chem. Phys.* **2011**, *13*, 2457−2487.

(40) Quinson, J.; Neumann, S.; Wannmacher, T.; Kacenauskaite, L.; Inaba, M.; Bucher, J.; Bizzotto, F.; Simonsen, S. B.; Kuhn, L. T.; Bujak, D.; Zana, A.; Arenz, M.; Kunz, S. Colloids for Catalysts: A Concept for the Preparation of Superior Catalysts of Industrial Relevance. *Angew. Chem., Int. Ed.* **2018**, *57*, 12338−12341.

(41) Beberwyck, B. J.; Surendranath, Y.; Alivisatos, A. P. Cation Exchange: A Versatile Tool for Nanomaterials Synthesis. *J. Phys. Chem. C* **2013**, *117*, 19759−19770.

(42) De Trizio, L.; Manna, L. Forging Colloidal Nanostructures via Cation Exchange Reactions. *Chem. Rev.* **2016**, *116*, 10852−10887.

(43) Fenton, J. L.; Steimle, B. C.; Schaak, R. E. Tunable intraparticle frameworks for creating complex heterostructured nanoparticle libraries. *Science* **2018**, *360*, 513−517.

https://doi.org/10.1021/acs.cgd.1c00165
Cryst. Growth Des. 2021, 21, 4299−4304

(44) The Co_3O_4 precursor is reduced to the metallic cobalt nanocomposite catalyst inside the reactor before performing FTS.
(45) Torres Galvis, H. M.; De Jong, K. P. Catalysts for Production of Lower Olefins from Synthesis Gas: A Review. *ACS Catal.* **2013**, *3*, 2130−2149.
(46) Dry, M. E. High quality diesel via the Fischer−Tropsch process − a review. *J. Chem. Technol. Biotechnol.* **2002**, *77*, 43−50.
(47) Bouchy, C.; Hastoy, G.; Guillon, E.; Martens, J. A. Fischer-Tropsch Waxes Upgrading via Hydrocracking and Selective Hydroisomerization. *Oil Gas Sci. Technol.* **2009**, *64*, 91−112.
(48) Dry, M. E. The Fischer−Tropsch process: 1950−2000. *Catal. Today* **2002**, *71*, 227−241.
(49) Cheng, Q.; Tian, Y.; Lyu, S.; Zhao, N.; Ma, K.; Ding, T.; Jiang, Z.; Wang, L.; Zhang, J.; Zheng, L.; Gao, F.; Dong, L.; Tsubaki, N.; Li, X. Confined small-sized cobalt catalysts stimulate carbon-chain growth reversely by modifying ASF law of Fischer−Tropsch synthesis. *Nat. Commun.* **2018**, *9*, No. 3250.
(50) Borg, Ø.; Dietzel, P. D. C.; Spjelkavik, A. L.; Tveten, E. Z.; Walmsley, J. C.; Diplas, S.; Eri, S.; Holmen, A.; Rytter, E. Fischer−Tropsch synthesis: Cobalt particle size and support effects on intrinsic activity and product distribution. *J. Catal.* **2008**, *259*, 161−164.
(51) The unknown density of the amorphous $Co(CO_3)_x(OH)_{2-2x}$ phase impedes a quantative correlation between the shrinking at the microscale and the exchange on the atomistic scale. Furthermore, IR spectroscopy suggests the presence of both carbonate and hydroxide groups (see Supporting Information).
(52) Gadow, R.; Kern, F. Pressureless Sintering of Injection Molded Zirconia Toughened Alumina Nanoparticles. *J. Ceram. Soc. Jpn.* **2006**, *114*, 958−962.
(53) Shirsath, S. E.; Kadam, R. H.; Gaikwad, A. S.; Ghasemi, A.; Morisako, A. Effect of sintering temperature and the particle size on the structural and magnetic properties of nanocrystalline $Li_{0.5}Fe_{2.5}O_4$. *J. Magn. Magn. Mater.* **2011**, *323*, 3104−3108.
(54) Iglesia, E. Design, synthesis, and use of cobalt-based Fischer-Tropsch synthesis catalysts. *Appl. Catal., A* **1997**, *161*, 59−78.
(55) Bezemer, G. L.; Radstake, P. B.; Koot, V.; Van Dillen, A. J.; Geus, J. W.; De Jong, K. P. Preparation of Fischer−Tropsch cobalt catalysts supported on carbon nanofibers and silica using homogeneous deposition-precipitation. *J. Catal.* **2006**, *237*, 291−302.
(56) Helmbrecht, L.; Futscher, M. H.; Muscarella, L. A.; Ehrler, B.; Noorduin, W. L. Ion Exchange Lithography: Localized Ion Exchange Reactions for Spatial Patterning of Perovskite Semiconductors and Insulators. *Adv. Mater.* **2021**, *33*, No. 2005291.

https://doi.org/10.1021/acs.cgd.1c00165
Cryst. Growth Des. 2021, 21, 4299−4304